Chapter 5

Phase Segregation Assisted Morphology Sculpting 2. Growth of Silicon via Vapor-Solid Reaction

5.1 Introduction

Various semiconductor nanostructures, such as nanoclusters, quantunm dots and nanowires, have attracted much attention in recent studies.[1-3]Among many semiconducting materials, silicon is the most important one for its wide applications in electronic, photonic, electrochemical and electromechanical devices.[4-8] In order to control the growth, many new synthetic strategies have been developed. For example, zero-dimensional (0D) silicon nanoparticles can be made by many methods, including gas phase decomposition of silanes, direct etching of silicon wafers, and solution reduction routes.[9-13] One-dimensional (1D) silicon nanowires have been prepared via vapor-liquid-solid (VLS) growth, laser ablation, and supercritical-fluid-liquid-solid (SFLS) synthesis.[14-18] Two-dimensional (2D) thin silicon nanosheets and nanobelts could been synthesized by thermal evaporation of silicon monoxide.[19] Also, porous silicon can be fabricated by etching silicon wafers in a solution of hydrofluoric acid.[20] Usually, the reported fabrication methods can only be applied to prepare silicon in limited examples of dimension and morphology. Previously, our group has reported that by employing simple vapor-solid reaction growth (VSRG) methods, many types of materials can be fabricated in the intrinsically anisotropic growth environment.[21-24] The unique features of VSRG are phase segregation and self-templating of the solid products. For example, using VSRG, silicon carbide can be fabricated into cubic shells and cages.[24] Recently, we have discovered that by reacting organoperchloro compounds with calcium carbide, which is another example of VSRG, porous, fibrous, and lamellar shaped

graphite materials can be produced easily at favorable reaction temperatures.[25] The phenomena are attributed to phase segregation and self-templating of the solid products, graphite and calcium chloride.[25] Comparable examples are found in natural mineralogy and block copolymer systems.[26,27] Here, we extend the exploration further and report a simple efficient VSRG method to fabricate crystalline silicon into many shapes. These include porous, clustered particulate, wire-like, flake-like, and lamellar structures. Below, we will discuss our discoveries.

5.2 Experimental Section

5.2.1 Synthesis

Mg_2Si (99.5 %) and $CaSi_2$ (95 %) were purchased from Strem and $SiCl_4$ (99 %) was obtained from Aldrich. In general, in a tubular reactor at 1023 - 1223 K 100 kPa, the silicide powder in an aluminum oxide boat was reacted with $SiCl_4$ evaporated at 255 K under bubbling Ar (5 sccm) for 16 h. The as-prepared products were further heat treated at 1073 K 0.13 Pa for 1 h to evaporate the chloride salts ($MgCl_2$ and $CaCl_2$). After the workup process, a purified product was collected.

5.2.2 Characterzation

Surface morphology of the products was directly examined by scanning electron microscopy (SEM, JEOL JSM-6330F at 15 kV). Energy dispersive X-ray spectroscopy (EDS) was used to confirm the element composition of the samples. Transmission electron microscopy (TEM, JEOL JEM-4000EX at 400 kV) was employed to evaluate microstructure of the products. X-ray diffraction (XRD, Bruker D8 Advance, Kα radiation at 40 kV and 40 mA) and Raman scattering spectroscopy (Jabin-Yvon Raman Spectrometer T-64000 with an incident wavelength at 514.5 nm) were employed to evaluate structural information and crystallinity of the products.

5.3 Results

From reactions between vaporized $SiCl_4$ and MSi_x, Mg_2Si and $CaSi_2$, at 1023 K - 1223 K and 1 atm, dark brown raw products were isolated. In Figure 5.1A-B, XRD study of the raw products showed co-existence of Si and hydroyzed MCl_2 salts in the solids.[28] The chloride salts can be sublimed at 1073 K to offer pure Si products, as supported by the reflections from (111), (220), (311), (400) and (331) lattice planes shown in the XRD patterns (Figure 5.2A-B). Thus, we conclude that the reactants were stoichiometricly converted into the products silicon and metal chlorides. A summary of the reactions, including stoichiometry, conditions and product morphology, is listed in Table 5.1.

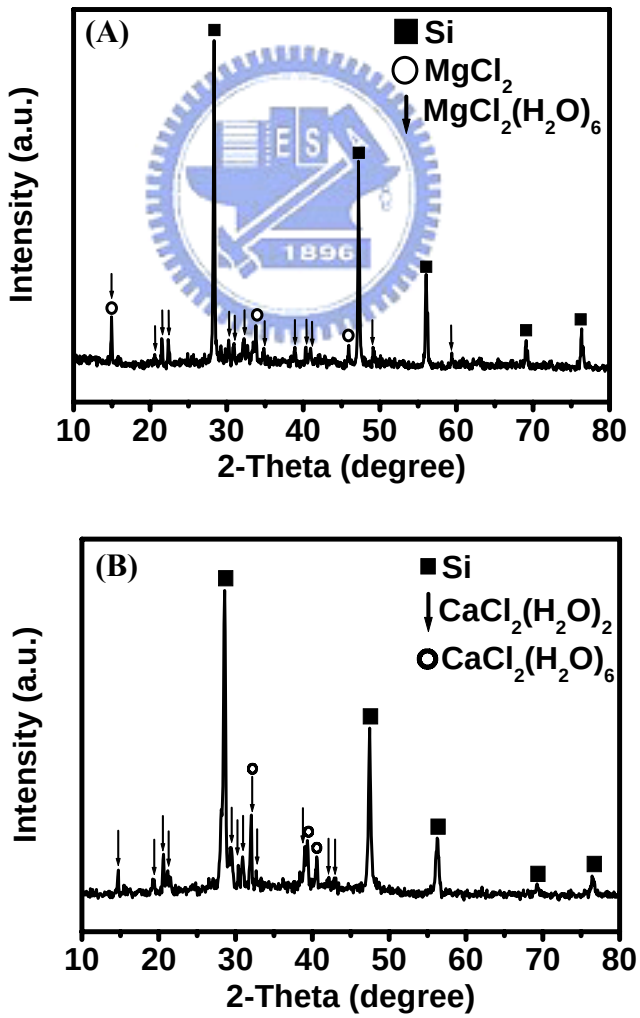

Figure 5.1 (A) XRD of silicon/$MgCl_2$/$MgCl_2(H_2O)_x$ product grown at 1123 K. (B) XRD of silicon/$CaCl_2(H_2O)_x$ product grown at 1123 K.

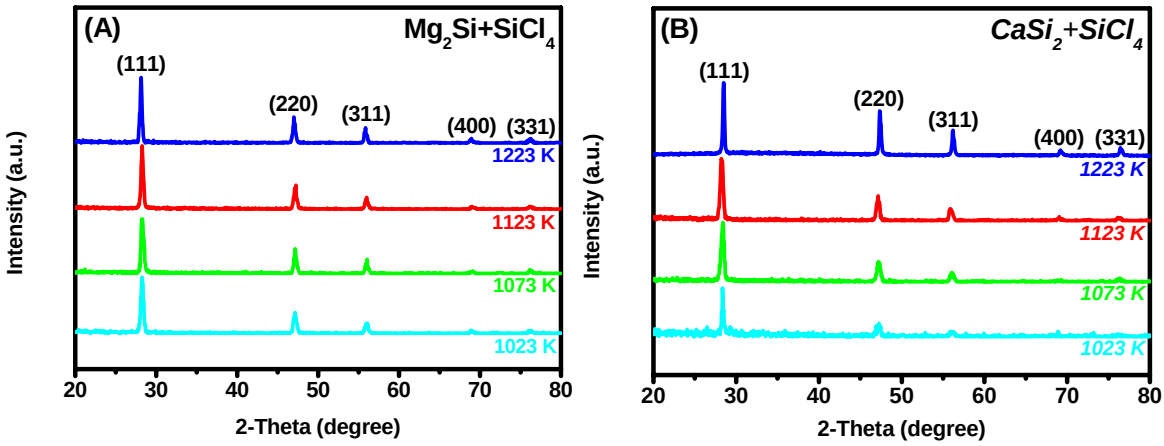

Figure 5.2 XRD of silicon products grown at 1023 K ─ 1223 K prepared from $SiCl_4$ reacted with (A) Mg_2Si ;(B) $CaSi_2$.

Table 5.1 Summary of morphology of silicon products obtained at different reaction temperatures.

1 Mg_2Si + 1 $SiCl_4$ → 2 Si + 2 $MgCl_2$	
Reaction Temperature (K)	Morphlogy
1023	**Clustered-particulate**. Diameter: one to few hundred nm; attached to neighboring ones.
1073	**Wire-like**. Diameter: 100 - 200 nm; length: up to tens μm.
1123	**Coral-like**. Trunk diameter: one to few hundred nm; branches with similar diameters.
1223	**Flake-like**. Flakes branched from wire-like trunk. Averaged flake length: up to several μm; averaged flake width: 200 – 800 nm; trunk diameter: several μm.
2 $CaSi_2$ + 1 $SiCl_4$ → 5 Si + 2 $CaCl_2$	
Reaction Temperature (K)	Morphology
1023	**Porous**. Irregular pores in irregularly shaped flakes. Pore sizes: 200 – 2000 nm.
1073	**Wire-like**. With protruded branches. Diameter: 50 - 100 nm; length: up to few μm.
1123	**Coral-like**. Trunk diameter: one to few hundred nm; branches with similar diameters.
1223	**Lamellar**. Thickness: 100 - 200 nm; diameter: up to μm.

5.3.1 Morphologies of silicon materials

SEM and EDS study of the raw products showed co-existence of Si and hydroyzed MCl_2 salts in the solids shown in Figure 5.3A-D. In Figure 5.4, morphology of several different products prepared from Mg_2Si and $SiCl_4$, after purification, is shown. We discovered that the product morphology changes dramatically as the reaction temperature changes. The product formed at 1023 K are clustered particles, as shown in Figure 5.4A. When the reaction temperature is increased to 1073 K, formation of nanowires is observed in Figure 5.4B. Figure 5.4C shows that coral-like products are generated at 1123 K. From the reaction temperature of 1223 K, flakes attached to nanowire stems are formed and can be seen in Figure 5.4D. Energy dispersive X-ray spectroscopy (EDS) proved that all of the products, regardless of their difference in morphology, are composed of silicon only. No other signals were found in the sample. This is consistent with the XRD data.

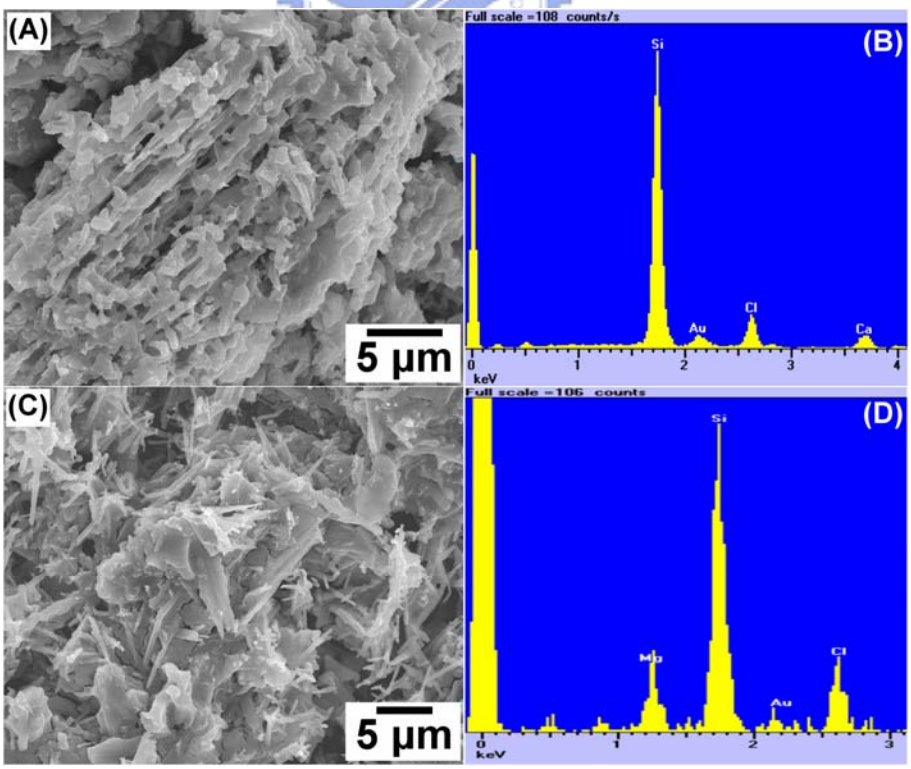

Figure 5.3 SEM and EDS silicon/$MgCl_2$ and silicon/$CaCl_2$ nanostructures synthesized from $SiCl_4$ and Mg_2Si, (A) SEM and (B) EDS of the as-prepared product grown at 1123 K; from $CaSi_2$, (C) SEM and (D) EDS of the as-prepared product grown at 1123 K.

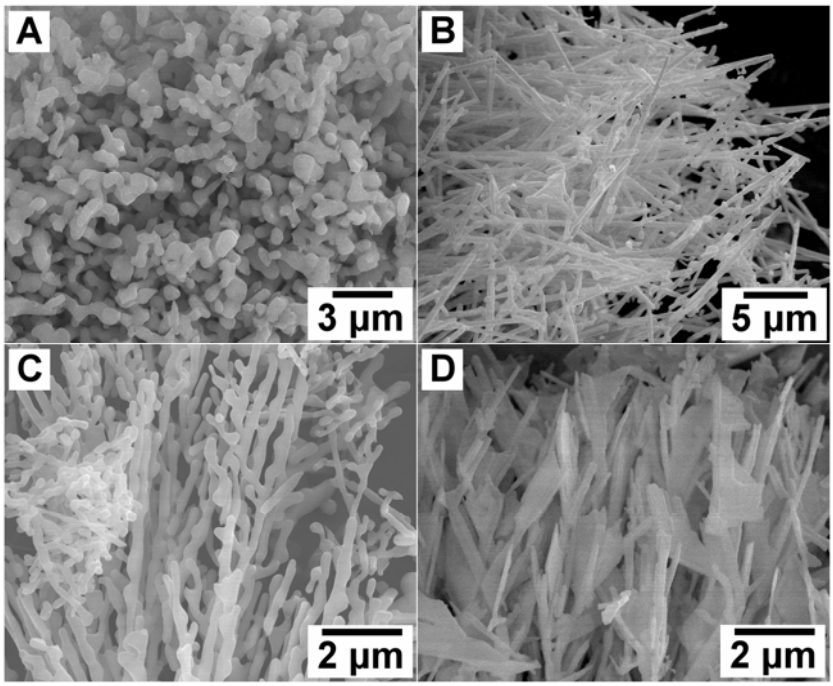

Figure 5.4 SEM images of silicon products prepared from Mg_2Si and $SiCl_4$. (A) Silicon particles, prepared at 1023 K; (B) silicon nanowires, prepared at 1073 K; (C) coral-like silicon, prepared at 1123 K; (D) flake-like silicon, prepared at 1223 K.

The products prepared from $CaSi_2$ and $SiCl_4$ are shown in Figure 5.5. The morphology of these products are similar to those synthesized by using Mg_2Si and $SiCl_4$. By simply varying the reaction temperature from 1023 K to 1223 K, the morphology changes from a porous structure (1023 K, Figure 5.5A), to branched nanowires (1073K, Figure 5.5B), to a coral-like structure (1123 K, Figure 5.5C), and finally to lamellar plates (1223 K, Figure 5.5D). EDS data also confirm that the products are composed of silicon. Our observation suggests that in this study, the reaction temperature is the most important factor to affect the product morphology. This parallels greatly to our previous study, fabrication of graphites with different morphology from the reactions between organoperchloro compounds and CaC_2.[25] In the study, we also observed that the reaction temperature affected the product morphology in a comparable way. As the reaction temperature was increased, the product morphology changed from a porous, to a fibrous, and finally to a lamellar structure.

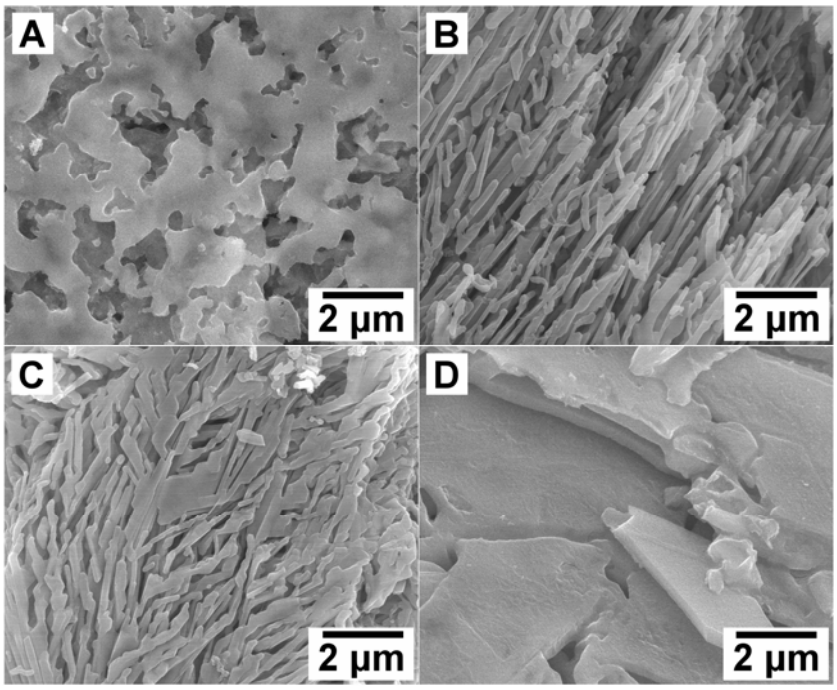

Figure 5.5 SEM images of silicon products prepared from $CaSi_2$ and $SiCl_4$. (A) Porous silicon, prepared at 1023 K; (B) silicon nanowires, prepared at 1073 K; (C) coral-like silicon, prepared at 1123 K; (D) lamellar silicon, prepared at 1223 K.

On the other hand, even the major features of the reactions are related, there are minor dissimilarities. The most apparent one is that in the cases of silicon growth, a unique coral-like morphology was observed. Even though the observed formation may be attributed to a transition between wire and lamellar structures, the possible reason for that silicon tends to branch may lie in its bonding preference. In general, silicon atoms favor sp^3 hybridized bonding arrangement in solid state. When conditions are appropriate, the stacking of silicon atoms may protrude from the main growth axis and into the coral-like morphology. On the other hand, graphite, with sp^2 hybridized carbon connections that form planar sheets of hexagonal networks, is more difficult to extend out unless less stabilized five or seven membered rings are formed.[29] Another interesting observation is that in the graphite case, porous structures were formed at 973 - 1023 K.[25] This parallels the reaction using $CaSi_2$ as the reactant at 1023 K. In the case, Si with a porous structure was also obtained (Figure 5.5A). On the other hand, clustered Si particles were synthesized from the

reaction employing Mg_2Si at the same temperature (Figure 5.4A). These observations suggest that the phase segregated reaction products, silicon and metal chlorides, may act as mold and cast to influence the final morphology. This is closely related to the graphite growth reported in the previous paper and will be discussed more below.[25]

5.3.2 Structural Characterization by TEM

The silicon materials were futher stucturally analyzed by using TEM. Figure 5.6 shows the images of the samples prepared from the reactions of $SiCl_4$ and Mg_2Si.

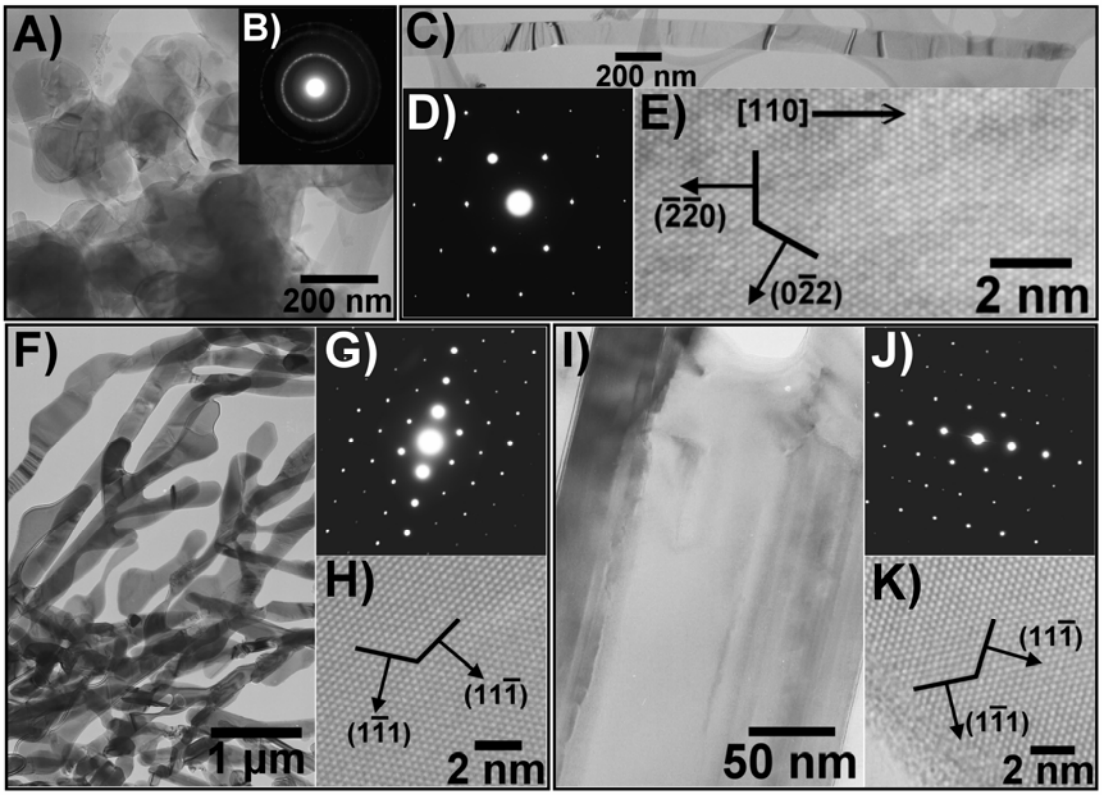

Figure 5.6 TEM studies of silicon products prepared from Mg_2Si and $SiCl_4$. (A) Low magnification and (B) SAED images of clustered silicon particles prepared at 1023 K. (C) – (E) Images of a single silicon nanowire prepared at 1073 K; (C) low magnification, (D) SAED along [-1 1 1] zone axis, and (E) high resolution. (F) – (H) Images of coral-like silicon prepared at 1123 K; (F) low magnification, (G) SAED along [0 1 1] zone axis, and (H) high resolution. (I) – (K) Images of flake-like silicon prepared at 1223 K; (I) low magnification, (J) SAED along [0 1 1] zone axis, and (K) high resolution.

Figure 5.6A displays that the particles prepared at 1023 K, with average diameters 150 – 300 nm, are clustered together. The selected area electron (SAED) in Figure 5.6B shows a pattern consiting (111), (200) and (311) rings of a cubic phase material. From the pattern, the lattice parameter *a* is calculated to be 0.547 nm, which is close to the value of bulk Si, 0.543 nm.[28] Figure 5.6C shows a low resolution image of a single flake-like silicon nanowire grown at 1073 K. The diamter of the nanowire ranges from 100 to 200 nm. The dot pattern in the ED study in Figure 5.6D suggets that the wire can be indexed to the [-1 1 1] zone axis of single crystal silicon. From the image, the lattice paprameter *a* is estimated to be 0.549 nm. Figure 5.6E shows a high resolution lattice image of the nanowire. The spacing between the parallel fringes from the crystalline structure was measured to be 0.192 nm. This is equal to the spacing of the {1 1 0} planes of silicon. The image also suggets that the defect-free single crystal nanowire grows along the [1 1 0] direction. A low-magnification TEM image in Figure 5.6F shows that the product grown at 1123 K is coral-like. The dot pattern in Figure 5.6G suggests that the sample is single crystalline and viewed along the [0 1 1] zone axis of Si. A high resolution image in Figure 5.6H suugets that the lattice fringes are spaced 0.31 nm apart. This distance coincides well with the {111} interplane distance of silicon. A TEM image shown in Figure 5.6I reveals a representative individual flake-like material in the sample prpared at 1223 K. The sample also presents a dot pattern in the ED study Figure 5.6J. This can be indexed to the [0 1 1] zone axis of cubic phase silicon. A high resolution image in Figure 5.6K reveals that the crystalline sample has a thin (< 1 nm) amorphous surface layer. The interlayer distance is 0.31 nm, identical to the {111} lattice plane distance of silicon. Figure 5.7 shows the TEM images of the samples prepared from the reactions of $SiCl_4$ and $CaSi_2$.

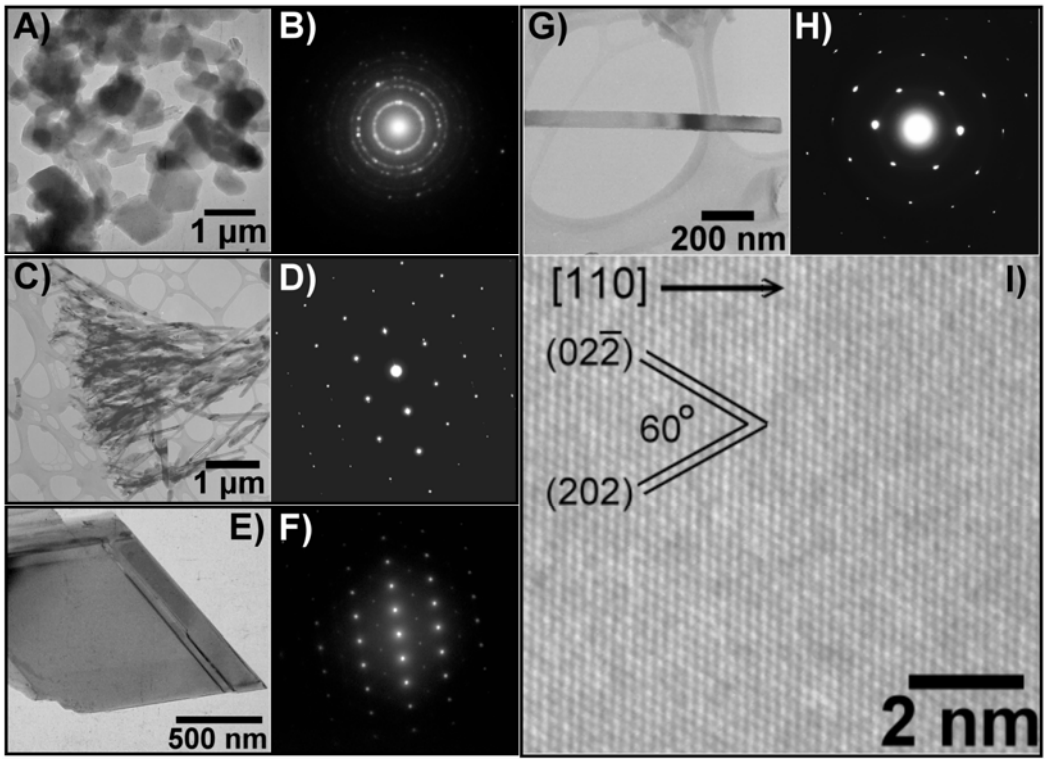

Figure 5.7 Varied morphology of silicon products prepared from $CaSi_2$ and $SiCl_4$. (A) TEM image and (B) SAED of porous structure prepared at 1023 K; (C) TEM image and (D) SAED taken along the [0 1 1] zone axis of coral-like silicon prepared at 1123 K; (E) TEM image and (F) SAED taken along the [1 -1 -2] zone axis of lamellar silicon prepared at 1223 K; (G) TEM (low magnification) image and (H) SAED taken along the [-1 1 1] zone axis and (I) HRTEM image of a single silicon nanowire prepared at 1073 K.

5.3.3 Structural Characterization by Raman

Raman scattering is very sensitive to lattice microstructures. Frequently, it is a useful tool to determine crystal symmetry of micro and nano crystalline materials. Here, Raman scattering was carried out to verify different silicon morphologies found in this study. In Figure 5.8, the results exhibit a prominent peak near 520 cm^{-1}, corresponding to the scattering of the first-order optical phonon of crystalline silicon.[30] For example, the clusted particles shows a symetric peak at 519.8 cm^{-1} in Figure 5.8A. As the size decreases and the morphology becomes more asymmetrical, probably due to an increase in structural defects, the peak downshifts and broadens asymmetrically. The observations are shown in Figures 5.8A – 5.8D and in Fiures 5.8E – 5.8H, for the cases using Mg_2Si and $CaSi_2$ respectively.

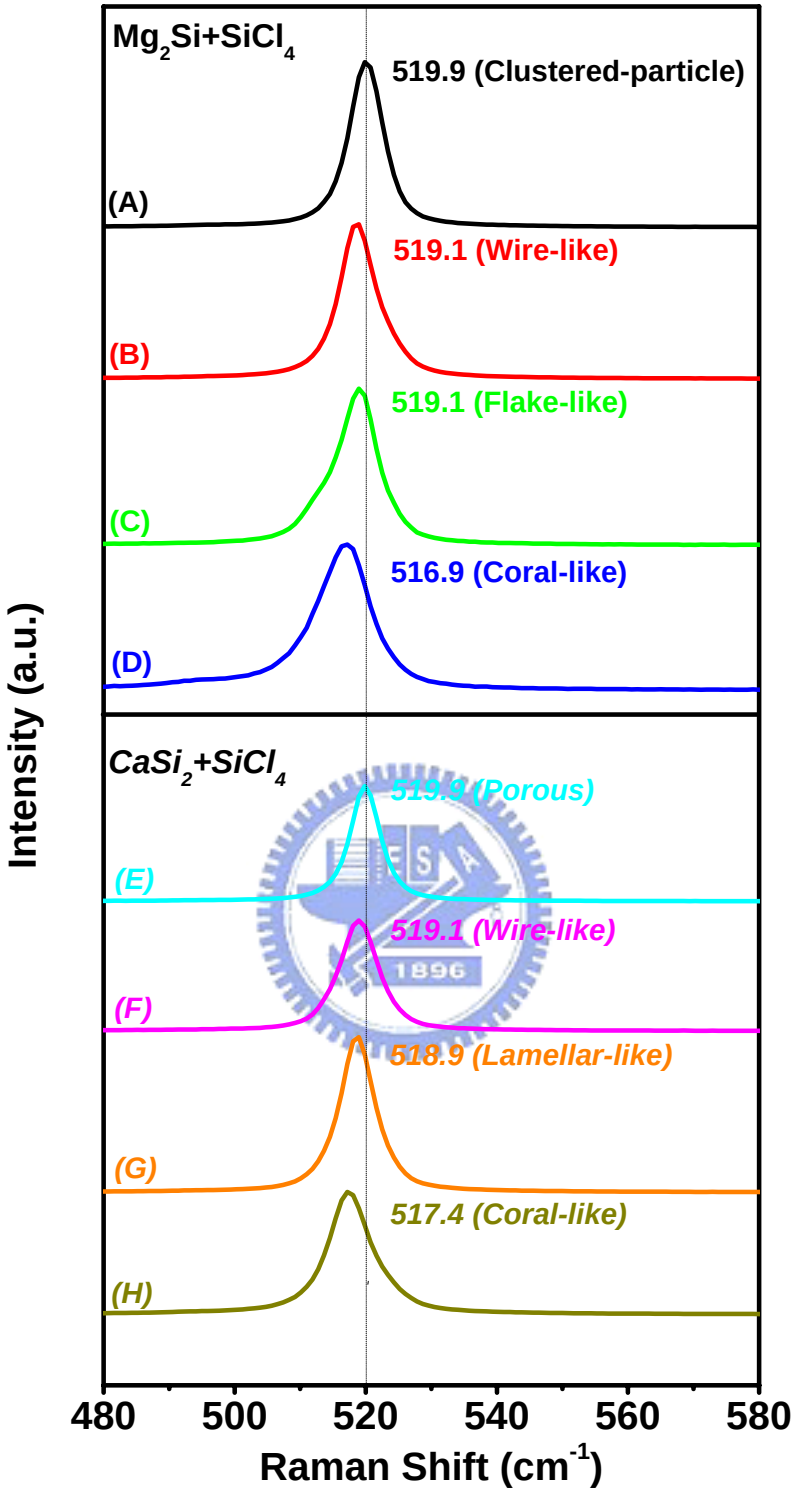

Figure 5.8 Raman spectra of the different structure silicon products prepared from $SiCl_4$ and Mg_2Si at (A) 1023 K, (B) 1073 K, (C) 1123 K, (D) 1223 K; and $CaSi_2$ at (E) 1023 K, (F) 1073 K, (G) 1123 K, (H) 1223 K.

In these, the coral-like structures, with more defects, show most significant shifts. Since nearly all structures have sizes greater than 20 nm, the down shift of the peaks at 520 nm was not caused by the size confinement effect. There is no signal observed for amorphous silicon (480 cm^{-1}), silicon dioxide (476 cm^{-1} and 460 cm^{-1}), and partially oxidized silicon (SiO_x) shell (signals between 400 cm^{-1} and 550 cm^{-1}), suggesting that the samples prepared in this study are highly purified crystalline silicon.[30-34]

5.4 Discussion

5.4.1 Morphology Alteration by Phase Segregation - Temperature effect

In this study, by varying the reaction temperature, we can fabricate silicon materials with various morphology from $SiCl_4$ and M_xSi_y (M= Mg, Ca). The reaction also generates MCl_2 salts as the other important product. Due to the difference of bonding interactions between Si and MCl_2, they do not dissolve each other according to "the like-dissolves-like rule". Consequently, caused by cohesive interactions, the products separate into different phases and perform the roles of mold and cast, which influence the product morphology cooperatively. To summarize our observations, in Scheme 5.1, a reaction pathway is illustrated. This highly parallels with the discovery saw in last chapter.[25] In the work, we showed that graphite materials of different morphology can be synthesized from C_xCl_y and CaC_2 at different temperatures also. At 973 - 1023 K. porous carbon was obtained. Fibrous carbon was synthesized at 1073 - 1123 K while planar carbon was grown at 1123 - 1223 K. The phase-segregated products graphite and $CaCl_2$ also acted as self-templating mold and cast to shape the product morphology at different temperatures. Strikingly, comparable product morphology is created at analogous temperature range in both cases. Despite the reactant and product the differences, there must be some common influential factors in them. One is that the ionic salt products $MgCl_2$ and $CaCl_2$ are relatively low melting 985 K and 1045 K, respectively.

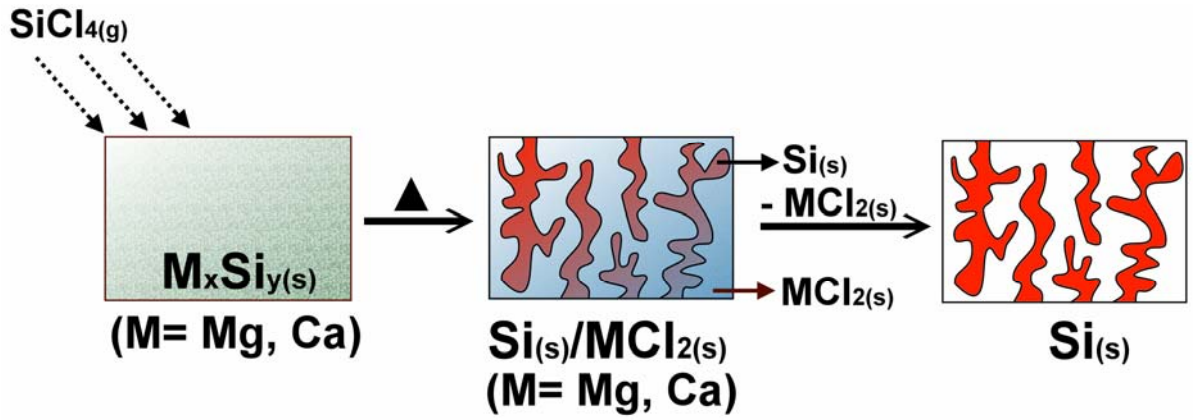

Scheme 5.1 An illustration of formation of textured silicon from $SiCl_4$ and metal silicides (metal = Mg, Ca).

This indicates that during the reaction, the salts were in free-flowing liquid states. The other is that both silicon and graphite products obtained in this and the last chapter are high melting network solids, 2683 K and 3948 K for Si and graphite respectively. The as-generated molecular level Si and C fragments probably solidify into the growing crystal lattice rapidly via an Ostwald ripening type process.[35] The crystallization process is also influenced by the other more fluidic salt product, which acted as the template to shape the final morphology of the products. The overall process can be rationalized that in order to minimize surface free energy, the as-formed nanoparticles would grow into a shape that tends to decrease the specific surface area. This leads to the formation of cluster-nanoparticles at low temperatures, cylinder-like structures. With increasing reaction temperature, the structure with more reduced surface energy is produced, from nanowire-like, then changing to coral-like, and finally to plate-shaped.

5.4.2 Morphology Alteration by Phase Segregation - Composition effect

The role of mold and cast shows a clear reverse for the samples prepared from Mg_2Si and $CaSi_2$ at 1023 K. The Si sample prepared from Mg_2Si shows a clustered-particle morphology (Figure 5.4A) while the product formed from $CaSi_2$ displays a porous morphology (Figure 5.5A). We attribute the phenomenon to the Si/salt molar volume ratio

of the products. From the reaction stoichiometry, the Si/$MgCl_2$ molar volume ratio from the reaction between Mg_2Si and $SiCl_4$ is 0.29 while the Si/$CaCl_2$ molar volume ratio from the reaction between $CaSi_2$ and $SiCl_4$ is 0.58. The observation suggests that the higher content component in the phase-segregated products forms the major framework while the lower content one embeds within it. Thus, in the first case, $MgCl_2$ formed the main structure while Si crystallized into the particles in that solid. In the second case, the higher silicon content caused Si to occupy more space in the solid and to be the host while the lower content $CaCl_2$ crystals were the guest encapsulated in it. After removal of the salts in both cases, the observed morphology is shown. In the previous study of graphite growth, formation of analogous porous structures was observed at 973 – 1023 K.[25] The C/$CaCl_2$ molar volume ratios ranged from 0.26 to 0.38, which is comparable to the Si/$CaCl_2$ molar volume ratio in this study. As the dimension of both products changed to 1-D and 2-D, the morphology difference of Si prepared from Mg_2Si and $CaSi_2$ diminishes, as shown in Figures 5.4B and 5.5B and in Figures 5.4D and 5.5D. The higher silicon content in the composition where is occupied more space in a unit cell cause porous structure shown in Figure 5.4A.

5.5 Conclusions

In this chapter, we report that from the VSRG reactions between $SiCl_4$ and MSi_x (Mg_2Si and $CaSi_2$), the products Si and MCl_2, with different surface energy, phase-segregate into mold and cast. Morphology of the products generated by the self-templating process depends on the reaction temperature and the product stoichiometry. These self-sculpting phenomenon parallels the growth of graphite with various morphology in the last chapter.[25] The observation found in these inorganic systems also show high resemblance to the morphology alteration frequently found in diblock-triblock copolymer systems.[27] The crystalline Si materials, prepared from the simple reactions in this study,

show surprisingly widely varying dimension scales including particle, porous, wire-like, coral-like, and lamellar shape. Their potential applications will be explored.

References

(1) Bley, R. A.; Kauzlarich, S. M. *J Am. Chem. Soc.* **1996**, *118*, 12461.

(2) Fuhrmann, B.; Leipner, H. S.; Hoche, H.-R.; Schubert, L.; Werner, P.; Gosele, U. *Nano Lett.* **2005**, *5*, 2524.

(3) Gray, J. L.; Atha, S.; Hull, R.; Floro, J. A. *Nano Lett.* **2004**, *4*, 2447.

(4) Huang, Y.; Duan. X.; Gui, Y.; Lauhon, L.; Kim, K. H.; Lieber, C. M. *Sceince* **2001**, *294*, 1313.

(5) Huang, H. M.; Mao, S.; Feick, H.; Yan, H. Q.; Wu, Y. Y.; Kind, H.; Weber, E.; Russo, R.; Yang, P. D. *Science* 2001, *292*, 1897.

(6) Huang, X. M. H.; Zorman, C. A.; Mehergany, M.; Roukes, M. L. *Nature* **2003**, *421*, 496.

(7) Lieber, C. M. *Sci. Am.* **2001**, *285*, 58.

(8) Prokes, S. M.; Wang, K. L. *MRS Bull.* **1999**, *24*, 13.

(9) Holmes, J. D.; Ziegler, K. J.; Doty, R. C.; Pell, L. E.; Johnston, K. P.; Korgel, B. A. *J Am. Chem. Soc.* **2001**, *123*, 3743.

(10) Belomoin, G.; Therrien, J.; Smith, A.; Rao, S.; Twesten, R.; Chaieb, S.; Nayfeh, M. H., Wagner, L.;Mitas, L. *Appl. Phys. Lett.* **2002**, 80, 841.

(11) Heath, J. R. *Science* **1992**, *258*, 1131.

(12) Kornowski, A.; Giersig, M.; Volgel, R.; Chemseddine, A.; Weller, H. *Adv. Mater.* **1993**, *5*, 634.

(13) Baldwin, R. K.; Pettigrew, K. A.; Ratai, E.; Augustine, M. P.; Kauzlarich, S. M. Chem. Commum. 2002, 1822.

(14) Gudihsen, M. S.; Wang, J.; Lieber, C. M.; *J. Am. Chem. Soc.* **2000**, *122*, 8801.

(15) Westwater, J.; Gosain, D. P.; Tomiya, S,; Usui, S.; Ruda, H. *J. Vac. Sci. Technol. B* **1997**, *15*, 554.

(16) Hu, J.; Odom, T. W.; Lieber, C. M. *Acc. Chem. Res.* **1999**, *32*, 435.

(17) Morales, A. M.; Lieber, C. M. *Science* **1998**, *279*, 208.

(18) Holmes, J. D.; Johnston, K. P.; Doty, R. C.; Korgel, B. A. *Science* **2000**, *287*, 1471.

(19) Shi, W.; Peng, H.; Wang, N.; Li, C. P.; Xu, L.; Lee, C. S.; Kalish, R.; Lee, S. T. *J. Am. Chem. Soc.* **2001**, *123*, 11095.

(20) Canham, L. T. *Appl. Phy. Lett.* **1990**, *57*, 1046.

(21) Yen, M.-Y.; Chiu, C.-W.;C.; Hsia, C.-H.; Chen, F.-R.; Kai, J.-J.; Lee, C.-Y.; Chiu, H.-T. *Adv. Mater.* **2003,** *15*, 235.

(22) Hsia, C.-H.; Yen, M.-Y.; Lin, C.-C.; Chiu, H.-T.; Lee, C.-Y. *J. Am. Chem. Soc.* **2003,** *125*, 9940.

(23) Huang, C.-H.; Chang, Y.-H.; Lee, C.-Y.; Chiu, H.-T. *Langmuir* **2006**, *22*, 10.

(24) Wang, C.-H.; Chang, Y.-H.; Yen, M.-Y.; Peng, C.-W.; Lee, C.-Y.; Chiu, H.-T. *Adv. Mater.* **2005**, *17*, 419.

(25) Huang, C.-H.; Lee, C.-Y.; Chang, Y.-H.; Peng, C.-W.; Chiu, H.-T. See in chapter 4.

(26) Brian, J.; Charles, F. K. *J. Sed. Petrol.* **1993**, *63*, 1018.

(27) Leibler, L. *Macromolecules* **1980**, *13*, 1602.

(28) The JCPDS number of XRD patterns: Si: 89-5012, $MgCl_2$: 89-1567, $MgCl_2(H_2O)_6$: 74-1039, $CaCl_2(H_2O)_2$: 70-0385, $CaCl_2(H_2O)_6$: 77-1782.

(29) Biro, L. P.; Bernardo, C.A.; Tibbetts, G. G.; Lambin, Ph. In *Carbon Filaments and Nanotubes: Common Origins, Differing Applications*; NATO Science Series: **2001**; p151-p153.

(30) Dapeng, B. L.; Zhang, S. L. *Phys. Rev. B* **1999**, *59*, 1645.

(31) Zhang, Y. F.; Tang, Y. H.; Wang, N.; Yu, D. P.; Lee, C. S.; Bello, I.; Lee, S. T. *Appl. Phys. Lett.* **1998**, *72*, 1835.

(32) Wang, N.; Tang, Y. H.; Zhang, Y. F.; Lee, C. S.; Bello, I.; Lee, S. T. *Chem. Phys. Lett.* **1999**, *299*, 237.

(33) Chi, W. S.; Peng, H. Y.; Zheng, Y. F.; Wang, N.; Shang, N. G.; Pan, Z. W.; Lee, C. S.; Lee, S. T. *Adv. Mater.* **2000**, *12*, 1343.

(34) Li, W. N.; Ding, Y. S.; Yuan, J.; Gomez, S.; Suib, S. L.; Galasso, F. S.; DiCarlo, J. F. *J. Phys. Chem. B* **2005**, *109*, 3291.

(35) Voorhees, P. W. *J. Statist. Phys*. **1985**, *38*, 231.